

Revisiting the Malvinas Current Upper Circulation and Water Masses Using a High-Resolution Ocean Reanalysis

Camila Artana¹ , Christine Provost² , Lea Poli² , Ramiro Ferrari³ , and Jean-Michel Lellouche¹ 

¹MERCATOR-OCEAN, Parc Technologique du Canal, Ramonville Saint Agne, France, ²Laboratoire LOCEAN-IPSL, Sorbonne Université (UPMC, Univ. Paris 6), CNRS, IRD, MNHN, Paris, France, ³CIMA/CONICET-UBA and UMI IFAECI-3351, Buenos Aires, Argentina

Key Points:

- The Malvinas Current is rather steady: Volume transport time series have little seasonality, no trend, and small relative standard deviations
- The upper 900 m transport mean decreases from 40 Sv at 51°S to 35 Sv at 41°S indicating offshore leakage along the MC path
- The Malvinas Plateau is a key region for water mass modification through eddy mixing and deep winter mixed layers

Supporting Information:

Supporting Information may be found in the online version of this article.

Correspondence to:

C. Artana,
cartlod@locean-ipsl.upmc.fr

Citation:

Artana, C., Provost, C., Poli, L., Ferrari, R., & Lellouche, J.-M. (2021). Revisiting the Malvinas Current upper circulation and water masses using a high-resolution ocean reanalysis. *Journal of Geophysical Research: Oceans*, 126, e2021JC017271. <https://doi.org/10.1029/2021JC017271>

Received 9 FEB 2021
Accepted 19 MAY 2021

Abstract We use 25 years of a high-resolution ocean reanalysis (1/12°) to revisit the Malvinas Current (MC) from the South (Drake Passage) to the North (Brazil-Malvinas Confluence) from the synoptic to interannual time scales. The Malvinas Plateau is home to active eddy mixing, eddy dissipation and deep winter mixed layers occasionally reaching 600 m depth. The MC is organized in two jets which merge around 44°S as the continental slope steepens. The upper 900 m transport mean decreases from 40 Sv at 51°S to 35 Sv at 41°S indicating offshore leakage along the MC path. The MC plays a minor role in the velocity variations observed at the Confluence at seasonal and interannual scales; those are driven by changes in the intensity of the Brazil Current over the slope (34–36°S). Computing MC transport time series at different latitudes requires care because the section eastern limits are embedded in an energetic region. Transport time series were produced at selected latitudes using different criteria and showed common features. They show little seasonality (relative seasonal standard deviation of 2%) and no significant trend. The MC is a steady current: the relative standard deviation is on the order of 10% increasing to 20% near and on the Malvinas Plateau and near the Confluence. In contrast, velocity trends are large in the Brazil Current with the overshoot migrating southward. The associated increase in mesoscale activity south of 44°S in the Argentine Basin might contribute to blocking events occasionally reducing the MC transport.

Plain Language Summary The Malvinas Current (MC) is a branch of the Antarctic Circumpolar Current and flows northward along the Patagonian slope. We revisit the MC upper circulation and water masses using a high-resolution ocean reanalysis from 1993 to 2017. The MC is a strong and rather steady current with little seasonality and no significant trend. The mean MC volume transport reduces from south to north by about 14%, indicating an offshore leakage along its path. The upper 500 m MC water underwent a freshening of 0.1 psu/decade.

1. Introduction

The Malvinas Current (MC), a major western boundary current of the South Atlantic, is the northernmost meander of the northern branch of the Antarctic Circumpolar Current (ACC), the Subantarctic Front (SAF). The North Scotia Ridge in Drake Passage (Figure 1a) acts as a barrier to the ACC fronts forcing the SAF and Polar Front (PF) branches to deviate to the north. The two SAF branches (SAF-N and SAF-M) cross the North Scotia Ridge west (600 m) and east (2,000 m) of Burdwood Bank (WBB and EBB, respectively), while the two northern branches of the PF (PF-M and PF-N) proceed through Shag Rocks Passage (3,200 m, SRP) (Figure 1a). Subsequently, the SAF branches cross the shallow Malvinas Plateau (<3,000 m) and continue their path northward forming the MC, while the PF follows an eastward path along the Malvinas Escarpment (Figure 1a). The MC is an equivalent-barotropic current that flows along the Patagonian continental slope with surface velocities of the order of 60 cm/s (Figure 1b). Observations suggest that the MC is organized in two narrow jets at 45°S (Frey et al., 2021; Piola et al., 2013). Poli et al. (2020) showed that shelf break trapped waves modulate the intensity of the inner jet -SAF-N branch- while slow waves propagating from the Malvinas Escarpment and the Drake Passage modify velocities in the main jet—SAF-M branch— (Figure 2a). The MC is concentrated in a narrow single jet at 41°S and encounters the Brazil Current (BC) at 38°S. Then part of the BC, referred to as the overshoot of the BC, flows southward and returns to the northeast at about 45°S while the MC splits in two branches: the inner branch keeps flowing northward sinking

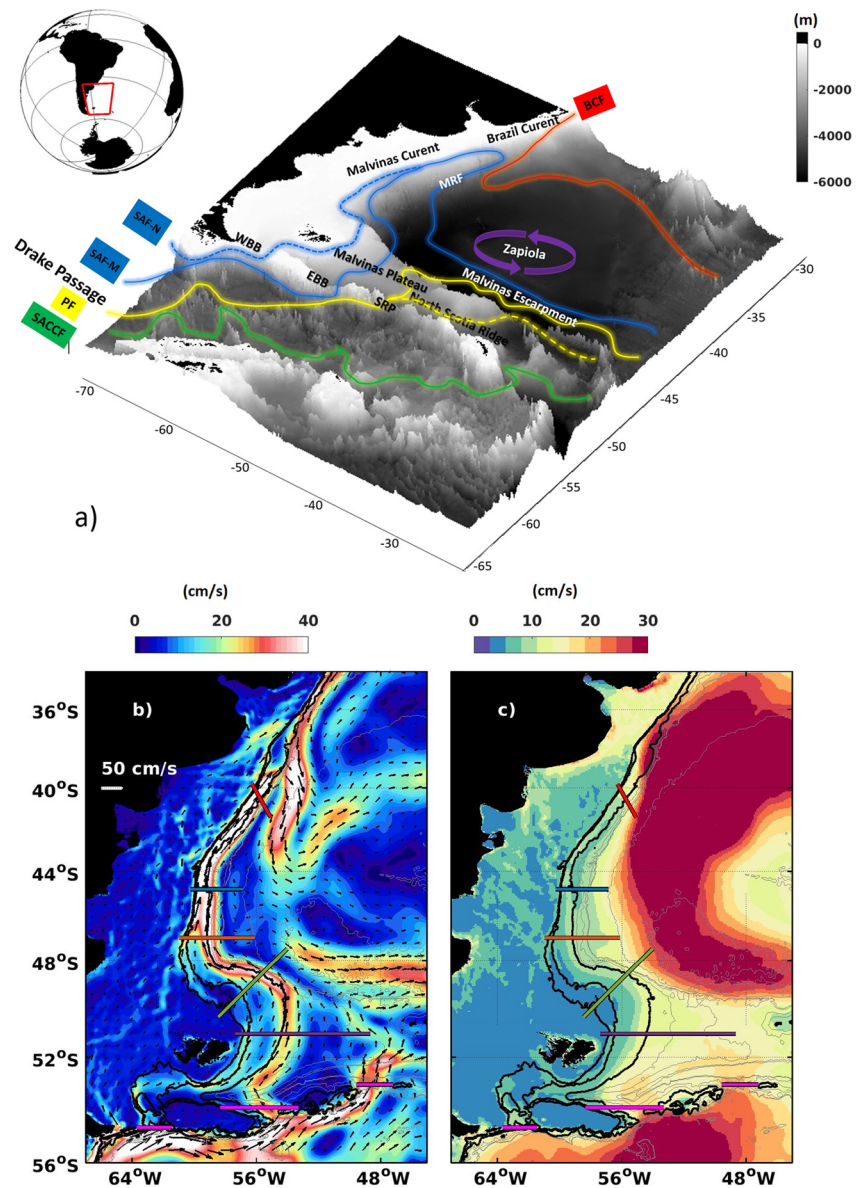


Figure 1. (a) Bottom topography of the Southwestern Atlantic and Drake Passage (in meters) from Smith and Sandwell (1994). The main passages through North Scotia Ridge are indicated: West of Burwood Bank (WBB), East of Burwood Bank (EBB), and Shag Rocks Passage (SRP). The mean location of the Antarctic Circumpolar Current fronts is schematized: Subantarctic Front (SAF-N and SAF-M, blue dashed and solid lines), Polar Front (PF-N and PF-M in yellow solid and dashed lines), and Southern ACC Front (SACCF, in green). The mean position of the Brazil Current Front (BCF) is indicated in red. (b) Mean surface velocities from 1993 to 2017 (in cm/s) from the ocean reanalysis (GLORYS12) documented in this study. (c) Square root of eddy kinetic energy over 25 years (in cm/s) from GLORYS12. In (b) and (c) the 300, 500 and 1,500 m isobaths are indicated with thick black contours and the 6,000, 5,000, 3,000, 2,000 with gray contours. Five sections crossing the MC at 41°S (red), 44.7°S (blue), 47°S (orange), 59°W (green), and 51°S (purple) and three sections at North Scotia Ridge, WBB, EBB, and SRP (magenta) are indicated.

below the BC while the outer branch describes a sharp cyclonic loop and returns southward (Artana, Provost, et al., 2019; Provost et al., 1995). The southward return flow is referred to as the Malvinas Return Flow (Peterson & Whitworth, 1989). The region of the confluence is known as the Brazil Malvinas Confluence and is associated with lateral temperature gradients as high as 1°C per 100 m (Barré et al., 2006; Gordon & Greengrove, 1986) and large meso and submesoscale eddies and filaments.

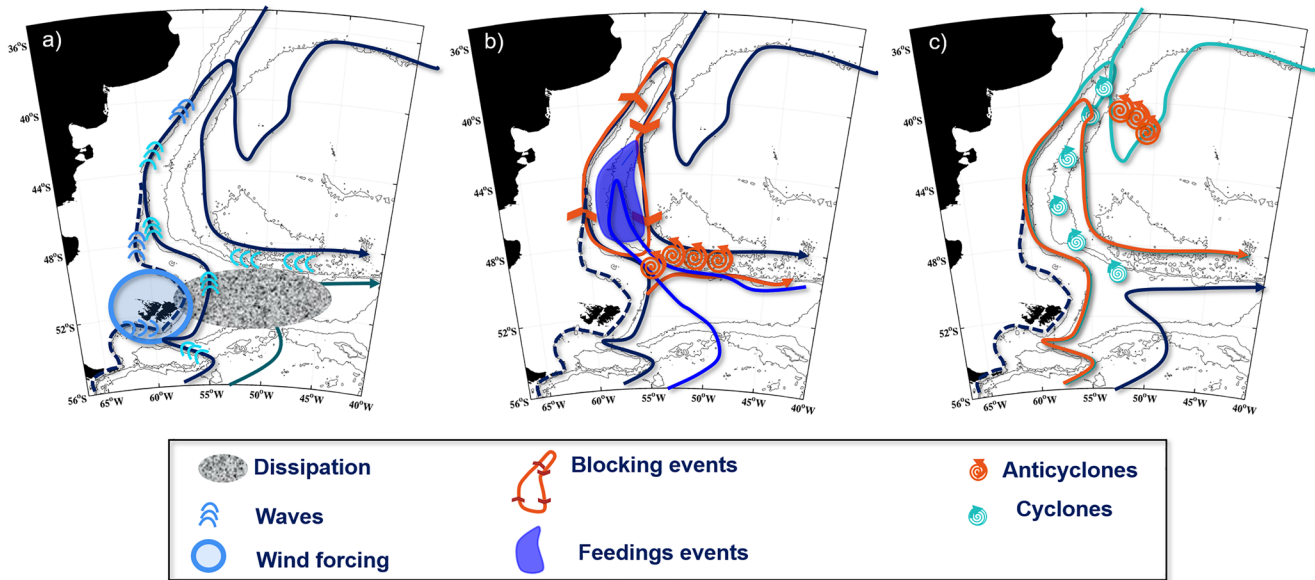


Figure 2. Schematics of physical processes in the MC based on previous studies. (a) Gray shading represents dissipation over the Malvinas Plateau of the mesoscale activity leaking through North Scotia Ridge (Artana et al., 2016). Trapped waves (locally wind forced and remotely forced) propagating along the Patagonian slope are schematized in blue (Poli et al., 2020). (b) Blocking events in red: anticyclonic anomalies cut the MC from the Antarctic Circumpolar Current at 49°S; the MC does not collapse as a recirculation cell is established (Artana et al., 2016, Artana, Lellouche, Sennechal, 2018). Feeding events in blue: waters from the South of the Polar Front are injected into the MC and recirculate between the MC and Malvinas Return Flow (Artana, Lellouche, Sennechal, 2018). (c) Maxima and minima of the MC transport at 41°S are associated with eddies coming from the Argentine Basin: Transport maximum cases (in blue) are associated with cyclonic eddies detached from the PF and transport minimum cases (in red) with southward displacement of the Subantarctic Front due to large anticyclonic anomalies from the Brazil Current (Artana, Ferrari, et al., 2018a).

Interestingly, although the MC presents moderate Eddy Kinetic Energy (EKE) values ($\sqrt{\text{EKE}}$ of 15 cm/s), it connects two of the most energetic oceanic regions: the Drake Passage ($\sqrt{\text{EKE}}$ of 30 cm/s) and the Brazil Malvinas Confluence ($\sqrt{\text{EKE}}$ of 45 cm/s, Figure 1c). Some of the Drake Passage EKE leaks across the North Scotia Ridge through the EBB and SRP and reduces over the Malvinas Plateau through dissipation and mixing (Artana et al., 2016, Figure 2a). As a result, $\sqrt{\text{EKE}}$ values over the Malvinas Plateau are in the order of 15 cm/s (Figure 1c). At the exit of the Malvinas Plateau, the MC is particularly exposed to mesoscale activity propagating westward along the Malvinas Escarpment. Around once a year the MC is cut from the ACC due to anticyclonic anomalies from the deep Argentine Basin (red in Figure 2b and Artana et al., 2016; Artana, Ferrari, et al., 2018). These blocking events are short-lived (from 10 to 35 days) and the MC downstream does not collapse rather becomes the western boundary of a recirculating cyclonic cell. Occasionally, the PF-N meanders north of the Malvinas Plateau and waters from the South of the Polar Front are injected into the MC as pulses or feeding events (blue in Figures 2b and Artana, Lellouche, et al., 2018). Polar waters accumulate in the recirculation region between the MC and the Malvinas Return Flow. Low-frequency variations in the water characteristics of the recirculation region are consistent with changes in the recurrence of feeding events.

The MC is the unique current in the southern hemisphere that carries Subantarctic Surface Water and Antarctic Intermediate Waters to latitudes as low as 38°S. These cold and nutrient rich waters are key for the development of rich ecosystems along the Patagonian shelf which sustain one of the largest fisheries of the world (Romero et al., 2006; Valla & Piola, 2015). The modification of water properties along the MC path is poorly understood and an evaluation of the MC transport over its latitudinal range is missing. To the date, the only volume transport time series of the MC have been produced at 41°S near the Brazil Malvinas Confluence where mooring data were gathered at different periods (Paniagua et al., 2018; Spadone & Provost, 2009; Vivier & Provost, 1999a). The mooring data were combined with satellite altimetry data to produce a 25 years-long transport time series in the upper 1,500 m (Artana, Ferrari, et al., 2018). Maxima and minima of the MC transport at 41°S were not associated with variations of the ACC, rather with eddies coming from the Argentine Basin: maxima were associated with cyclonic eddies detached from the Polar

Front (in blue in Figure 2c) and minima with large anti-cyclonic anomalies from the Brazil Current (in red in Figure 2c).

Here, we revisit the MC from its southern part to its northernmost tip from synoptic to interannual time scales using 25 years of the high-resolution Mercator Ocean reanalysis GLORYS12. This reanalysis has shown skills in reproducing the hydrography and circulation of the Argentine Basin in the upper layers and proved to be a most valuable tool to study the MC in this region where in situ observations are rather scarce (Artana, Lellouche, Park, et al., 2018, Artana, Lellouche, Sennechael, et al., 2018, Artana, Provost, et al., 2019; Poli et al., 2020). We aim at assessing the MC transport at different latitudes and at documenting modification of MC water properties. We focus on the upper circulation and upper water masses of the MC all along its path. After a presentation of the reanalysis and its evaluation (Section 2), we investigate the velocity structure along the continental slope and produce volume transport time series in the upper 900 m at different latitudes (Section 3). Modifications of the Subantarctic Surface Water and Antarctic Intermediate Waters are examined in Section 4 and their volume transport evolutions in Section 5. Results are summarized in Section 6.

2. Mercator Ocean Reanalysis

2.1. Description of the GLORYS12 Reanalysis

We use daily means of 25 years (1993–2017) of high-resolution ($1/12^\circ$) global Mercator Ocean reanalysis (hereafter, GLORYS12) from Copernicus Marine Environment Monitoring Service (CMEMS, <http://marine.copernicus.eu/>). GLORYS12 is based on the current real-time global high-resolution forecasting CMEMS system PSY4V3 (Lellouche et al., 2018). Compared to PSY4V3, GLORYS12 reanalysis uses the reprocessed atmospheric forcing coming from the global atmospheric reanalysis ERA-Interim and benefits from a few changes in the system settings about observation errors. The model has 50 vertical levels with 22 levels in the upper 100 m leading to a vertical resolution of 1 m in the upper levels and 450 m at 5,000 m depth. The physical component of the model is the Nucleus for European Modeling of the Ocean platform (NEMO). The model assimilates observations using a reduced-order Kalman filter with a 3-D multivariate modal decomposition of the background error and a 7-days assimilation cycle (Lellouche et al., 2013). Along-track satellite altimetric data from CMEMS (Pujol et al., 2016), satellite sea surface temperature from NOAA, sea-ice concentration, and in situ temperature and salinity vertical profiles from the latest CORA in situ databases (Cabanès et al., 2013; Szekeley et al., 2016) are jointly assimilated. A 3D-VAR scheme provides an additional 3-D correction for the slowly evolving large-scale biases in temperature and salinity when enough observations are available (Lellouche et al., 2018).

2.2. GLORYS12 Evaluation in the Southwestern Atlantic and Drake Passage

In a previous work, Artana, Lellouche, Park, et al. (2018) evaluated the performance of PSY4V3 in the Southwestern Atlantic Ocean. Ten years (2007–2016) of model outputs were compared to assimilated satellite and Argo float data and to independent in situ data that were not assimilated. The comparison showed that the PSY4V3 system correctly reproduces the general circulation and the complex hydrographic features of the Southwestern Atlantic Ocean upper layers. The authors found an excellent agreement between model and satellite sea surface height (Artana, Lellouche, Sennechael, et al., 2018). In a subsequent work general agreement between GLORYS12 and PSY4V3 was found, and comparisons with observations showed that GLORYS12 is closer to the data than PSY4V3 in the region of interest (Artana, Lellouche, Sennechael, et al., 2018).

An extensive evaluation of GLORYS12 velocities was also performed at Drake Passage (Artana, Ferrari, et al., 2019). GLORYS12 velocities compared well with independent current meter data in the water column and 50 m above the seafloor. The GLORYS12 total ACC volume transport has a mean of 155 (3 Sv being the uncertainty on the mean) and a standard deviation (std) of 6.7 Sv over 25 years (Artana, Ferrari, et al., 2019).

Here, we focus on the upper MC as GLORYS12 performance was only evaluated in the upper layers of the Southwestern Atlantic Ocean. We tentatively examined the stream function of the mean volume transport between the surface and the bottom in the Southwestern Atlantic Ocean: the total MC transport decreases

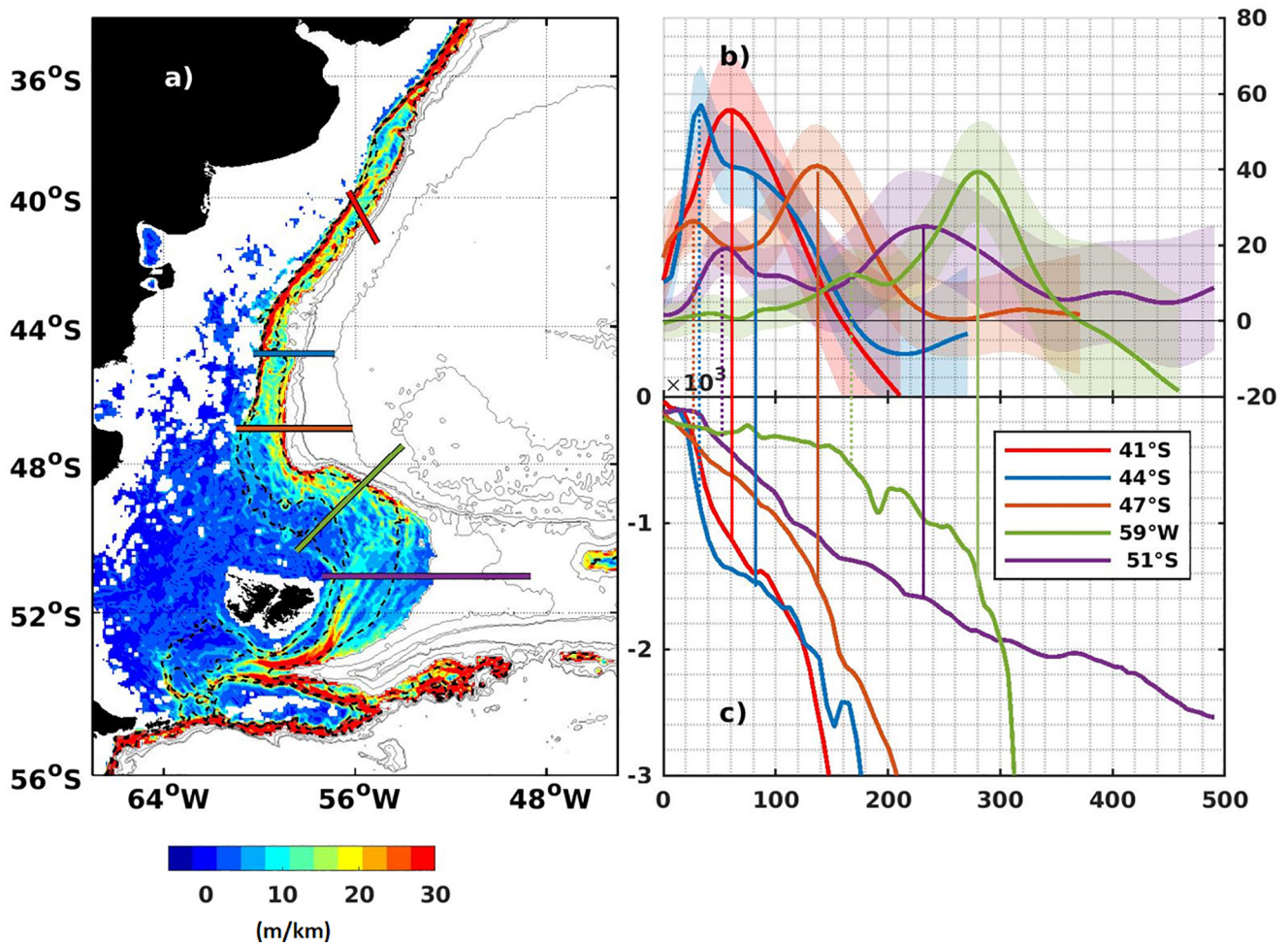


Figure 3. (a) Bathymetry gradient (m/km). Dashed lines indicate the 300, 500, and 1,500 m isobaths. (b) Mean along-slope surface velocities in cm/s along five sections crossing the MC at 41°S (red), 44.7°S (blue), 47°S (orange), 59°W (green), and 51°S (purple) (indicated in a). Shaded areas correspond to the velocity std. X-axis is distance in km from isobath 100 m. (c) Bathymetry along the same sections (same color code). Y-axis is depth in meters. Solid and dashed vertical lines indicate the location of maximum velocities of the offshore (SAF-M) and inshore (SAF-N) jets.

from 75 Sv at 51°S to 55 Sv at 47°S and 50 Sv at 44.7°S and 41°S. These values are consistent with the few total volume transport estimates derived from in situ data (Colin de Verdière & Ollitrault, 2016; Maamaatuaiahutapu et al., 1998; Peterson, 1992; Saunders & King, 1995) (see supplementary material S1).

3. The MC Upper Circulation

3.1. Surface Velocity: Mean and Variations

The MC mean surface velocity structure evolves with the continental slope geometry (Figures 1b and 3). At 51°S, over the Malvinas Plateau, the slope is gentle (8 m/km), the mean MC organized in two rather wide jets (150 and 200 km, purple in Figure 3b) centered on local gradient bathymetry maxima (10 m/km) located on the 400 and 1,500 m isobaths. The inner (20 cm/s) and offshore jets (25 cm/s) are associated with the SAF-N and the SAF-M respectively. Further east, a smaller jet (8 cm/s) above the 2,000 m isobath corresponds to the northern branch of the PF. Further north, as the slope steepens, the jets narrow, intensify and then merge around 44°S (Figure 1b). Between 51°S and 46°S, the offshore jet is located above the 1,500/1,400 m isobath while the inshore jet follows the shelf break which varies between 300 and 500 m (green and orange sections in Figure 3). The mean surface velocity of the offshore jet increases toward the north ranging from 25 cm/s at 51°S to 40 cm/s at 47°S. In general, the mean surface velocities of the offshore jet are twice as large as those of the inshore jet. However, at 44.7°S where the MC transitions to a single jet

regime as the slope steepens (30 m/km), the two jets merge and the largest surface velocities (58 cm/s) are found above 200 m (blue section in Figure 3). This is consistent with mean surface velocities derived from the mean dynamic topography from Mulet et al. (2020) (see supplementary material S2) and a month-long record of ADCP observations above the 200 m isobath at 44.7°S which documented velocities as large as 68 cm/s at 20 m depth (Saraceno et al., 2020).

Overall, the MC is a rather stable current with surface velocities presenting relatively homogeneous and small stds (10 cm/s, Figures 1c and 3b). Std of the surface velocity is larger in the outer part of the sections, in particular at 51°S, 59°W, and 41°S (~15 cm/s, Figure 3b), which are under the influence of offshore perturbations (Figure 1c). The impact of the offshore mesoscale activity on the MC surface velocities is illustrated in a synoptic situation in the supplementary material S3.

Surface velocities do not change in the MC at seasonal time scale while they increase by 15 cm/s in summer at the BC and Brazil Malvinas Confluence (Figures 4a and 4b). The overshoot is located 3° further south in winter (44°S–54°W) than in summer. The velocities in the overshoot are larger in winter (+15 cm/s) suggesting that the BC summer intensification advects into a winter intensification of the overshoot. The SAF remains at a similar position regardless of the season and the Subtropical Front pivots over a point located at 38°S over the slope (1,000 m isobath) as observed in Saraceno et al. (2004). In relation with the overshoot seasonal displacement, the offshore EKE shows large values further south in winter (not shown).

Surface velocity trends over the 25 years are relatively small, although significant in the MC, with a weakening (−2 cm/s/decade) in the inshore part of the MC and a strengthening in the offshore part (2 cm/s/decade) possibly indicating an offshore displacement of 20 km (Figure 4c). The surface velocity trend also suggests a small shift in the position of the northern branch Polar Front over the Malvinas Plateau of 60 km westward. Interestingly the EKE surface trends are positive over EBB and the eastward flank of SRP (50 cm²/s²/decade) suggesting an increase of the EKE leakage toward the Malvinas Plateau.

Surface velocity trends over the slope are large around 38°S (10 cm/s/decade) and reflect the southward displacement of the confluence associated with an intensification of the southward flow of the BC as observed in Artana, Provost, et al. (2019a). The large cyclonic structure centered at 55°W–43°S in the surface velocity trend indicates a southward displacement of the BC overshoot with an intensification of the surface velocities south of 44°S (Figure 4c). As a result, the EKE trends are positive and large (150 cm²/s²/decade) in the southward part of the Argentine Deep Basin (Figure 4d).

The MC presents a barotropic equivalent structure (Vivier & Provost, 1999b) and the features at depth are consistent with those observed at the surface as shown in the stream function of the mean volume transport in the upper 900 m (Figure 5).

3.2. Volume Transport in the Upper 900 m

The MC mean transport in the upper 900 m at 44.7°S is about 37 Sv with a contribution of 3 Sv from WBB, 23 Sv from EBB, and 11 Sv from SRP (Figure 5a, transport streamlines every 5 Sv). About two thirds of the full SRP transport follow the PF, turn eastward and do not reach 44.7°S. Near the Confluence, at 41°S the mean MC transport (35 Sv) is larger than the BC mean transport (20 Sv at 36°S). The upper 900 m transport does not change with seasons over the MC while it increases by 10 Sv over the BC in summer and by 5 Sv over the overshoot in winter (Figures 5b and 5c) in agreement with the surface velocity seasonality discussed in Section 3.1. The transport seasonal behavior is robust: seasonal averages computed over different years yield similar results (not shown).

The MC transport does exhibit variations at interannual scale. As an example, we show the mean transports in 2015 and 2003 which correspond, respectively, to small (30 Sv) and large (40 Sv) values at 41°S (Artana, Ferrari, et al., 2018, Artana, Provost, et al., 2019). Interestingly the MC transport upstream, between 48 and 42°S, is 5 Sv larger than the mean in 2015 and similar to the mean (35 Sv) in 2003 (Figures 5d and 5e). This example illustrates that the transport variations at 41°S do not reflect upstream MC transport changes rather local perturbations near the Confluence (as schematized in Figure 2c). Indeed, anticyclones from the overshoot reduced the transport by 5 Sv at 41°S in 2015, while in 2003 cyclones from the south advected offshore over the 4,000 m isobath locally reinforce the MC transport when they reached 41°S (Figures 5d

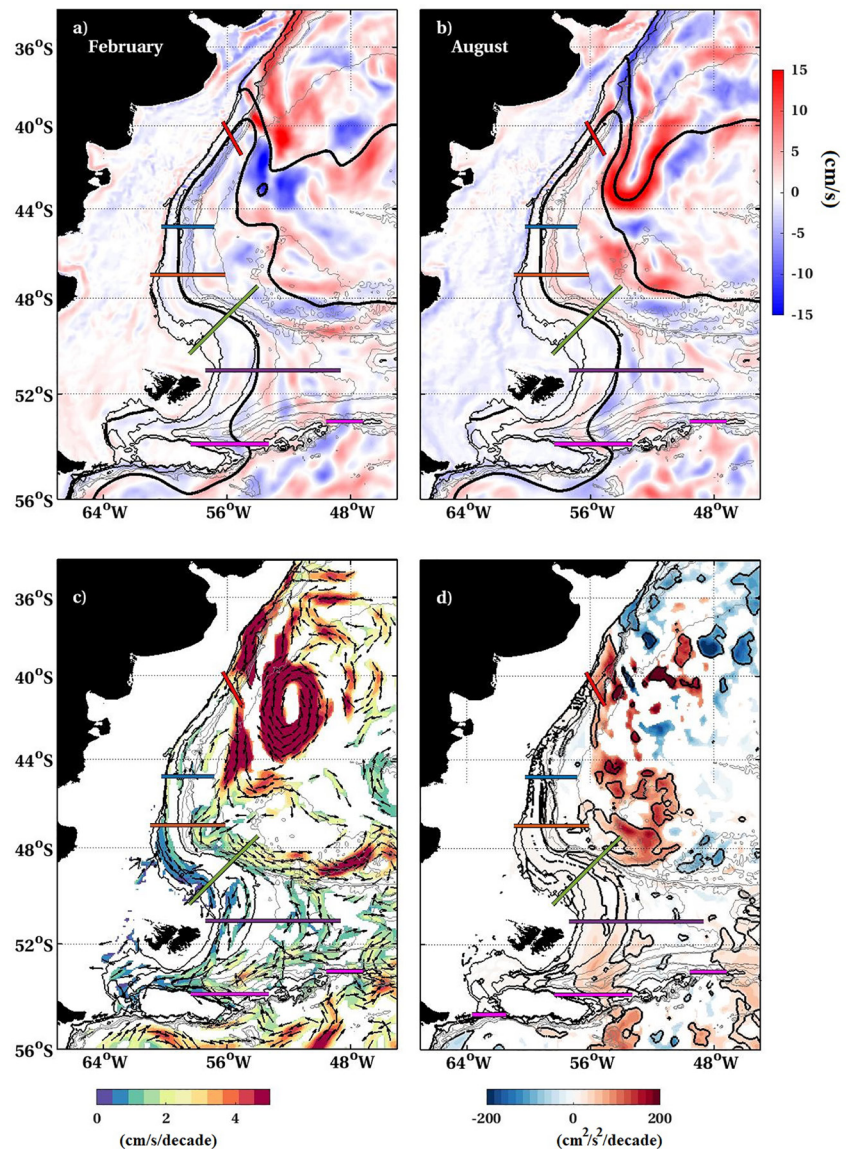


Figure 4. Surface velocity anomalies over 25 years (in cm/s) in February (a) and August (b). The mean position of the Subantarctic Front (Sea Surface Height = -5 cm) and Brazil Current Front (Sea Surface Height = 30 cm) are indicated in black contours. (c and d) Significant linear trends (above the 95% confidence level) in surface velocity (cm/s/decade) and EKE ($\text{cm}^2/\text{s}^2/\text{decade}$) computed over 25 years (1993–2017). The black contour delineates points where the 25-years trend is larger than the std. Isobaths as in Figure 1. Five sections crossing the MC at 41°S (red), 44.7°S (blue), 47°S (orange), 59°W (green), and 51°S (purple) three sections at North Scotia Ridge (in magenta) are indicated.

and 5e; Artana, Lellouche, Sennechael, et al., 2018). The return flow of the MC shows different behaviors in 2003 and 2015. While in 2003 the Malvinas Return Flow flows straightforward south toward the Malvinas Escarpment, in 2015 part of the Malvinas Return Flow turns northwestward following the BC overshoot.

MC volume transport time series in the upper 900 m were estimated at five latitudes in different ways to account for the difficulty in defining an eastern boundary to the sections. Indeed, if the section western boundary is straightforward, taken here as the 100 m isobath, the eastern limit is open and lies in an energetic environment. Sensitivity tests to the length of the sections were performed (extending and reducing the section length by 50 km). Volume transports time series were estimated considering positive ($T+$) and both sign velocities ($T\pm$). The times series are presented in supplementary material S4 and their statistics in Table 1. From now on we only examine ($T+$) and ($T\pm$) are highly correlated (the lowest

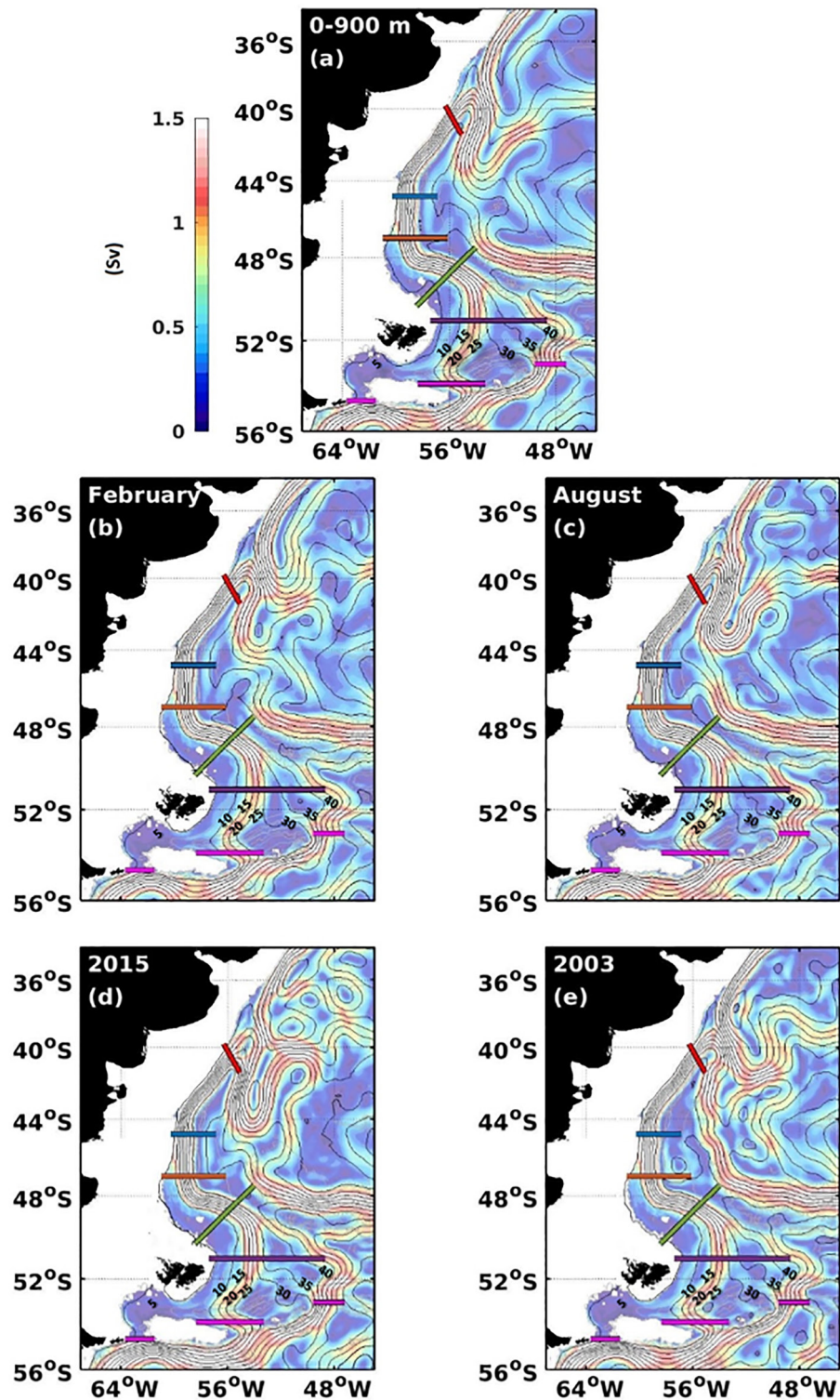


Figure 5. Mean transport stream functions computed between surface and 900 m depth over 25 years (a), over the 25 months of February (b) and August (c), over full year 2015 (d) and full year 2003 (e). Streamlines are plotted every 5 Sv. Background is mean volume transport (in Sv) in each model grid (transport density). Five sections crossing the MC at 41°S (red), 44.7°S (blue), 47°S (orange), 59°W (green), and 51°S (purple) and three sections at North Scotia Ridge (in magenta) are indicated.

Table 1

Statistics of the Upper 900 m Volume Transport Computed Considering Only Positive (T_+) and all Velocities (T_{\pm}) Across 5 Sections Crossing the MC at 41°S, 44.7°S, 47°S, 59°W, and 51°S and 3 Sections at North Scotia Ridge: At EBB, WBB, and SRP (Location Indicated in Figure 1c)

Section	Upper 900 m volume transport (T_+)/(T_{\pm})						r
	Mean (Sv)	Std (Sv)	Mean seasonal range (Sv)	Interannual range (Sv)	Synoptic max (Sv)	Synoptic min (Sv)	
41°S	37/30	8/13	5/7	14/30	65/65	2/−25	0.86
44.7°S	38/29	4/8	3/4	6/16	54/52	25/−7	0.62
47°S	42/37	4/6	5/5	5/8	60/58	27/13	0.80
59°W	45/35	9/15	5/8	9/13	95/95	17/−20	0.85
51°S	40/34	6/9	3/4	8/8	68/57	24/8	0.73
EBB	23/20	6/6	4/4	7/6	57/55	7/4	0.86
SRP	31/30	7/7	5/5	9/10	55/55	6/0	0.91
WBB	3/1	1/1	1/1	1/1	7/6	0/−1	0.97
EBB +SRP+WBB	57/51	8/8	7/4	9/7	93/90	33/22	0.92

The correlation coefficient (r) between transport time series computed from T_+ and T_{\pm} is reported in the last column.

correlation of 0.62 observed at 44.7°S results from the recurrent southward flow of the Malvinas Return Flow impinging on the eastern part of the section) and (T_+) means are closer to the mean values shown in Figure 5a (being 6–10 Sv larger than [T_{\pm}]). As expected, the std is largest (>8 Sv) at 41°S, 59°W, and 51°S sections where the offshore side of the sections reaches a large EKE region (Table 1, Figure 1c). Correlations between transport time series from different latitudes are significant (above the 99% confidence level) although relatively small because of the local mesoscale activity on the eastern boundary of each section (Table 2). The upper 900 m transport time series at EBB and SRP are not correlated with the transport of the sections located further north. This is consistent with Artana et al. (2016) who showed that an important part of the mesoscale activity coming from Drake Passage is damped out over the Malvinas Plateau (Figure 2a). The range of variations at synoptic scale is of the order of 30 Sv. The transport varies over a relatively small range at seasonal scale (<5 Sv on average) in contrast to the larger interannual variations (range larger than 10 Sv on average).

The MC carries several water masses that we examine focusing on their temporal and spatial distribution, their modification and long-term changes.

Table 2

Correlations Between the Transport Time Series at Different Latitudes

	41°S	44.7°S	47°S	59°W	51°S
41°S		0.13	0.15	0.11	0.12
		0.59	0.27	0.16	0.17
44.7°S			0.30	0.16	NS
			0.54	0.30	0.20
47°S				0.37	0.12
				0.44	0.21
59°W					0.14
					0.18

In each box, the first line corresponds to the volume transport in the upper 900 m, the second line to the MUW volume transport. Both transport time series were computed only considering positive velocities.

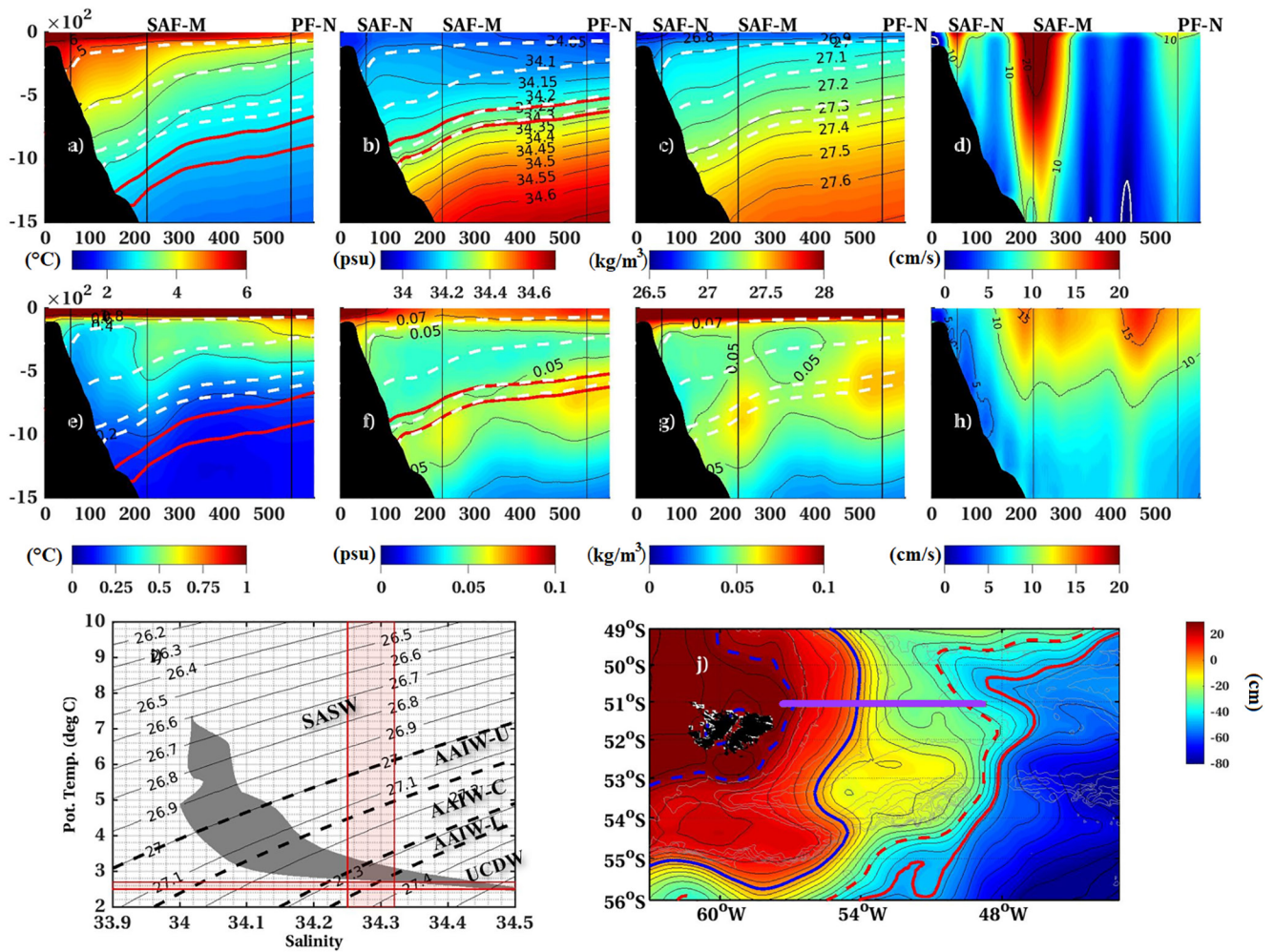


Figure 6. (a–d) Mean and (e–h) std of potential temperature (°C), salinity (psu), density (kg/m³), and along slope velocities from GLORYS12 (1993–2017) along the Patagonian slope at 51°S (purple section in j). X-axis in km from the 100 m isobath and Y-axis is depth in m. The 2.5°C isotherm and 34.25 psu isohaline are indicated in red, the 27.00, 27.14, 27.29, 27.35 kg/m³ isopycnal in dashed white. (i) Corresponding mean Θ -S diagram. The vertical rectangle marks 34.25 and 34.32 psu values and the horizontal rectangle the 2.5°C and 2.7°C values. (j) Mean Sea Surface Height (in cm) over 25 years. The SAF-N/SAF-M and PF-N/PF-M are indicated in solid/dashed blue and red lines, respectively.

4. Water Masses in the MC

Following Maamaatuaiahutapu et al. (1994), several water masses are identified at 51°S (Figures 6a–6c). The mean temperature and salinity of the upper 100 m (4.8°C and 34.05 psu) correspond to the light Subantarctic Surface Water (SASW; $\sigma_\theta < 27.00$ kg/m³). Below, three varieties of AAIW can be distinguished (Provost et al., 1995): the light upper AAIW (AAIW-U) ($27.00 < \sigma_\theta < 27.14$ kg/m³), a central AAIW (AAIW-C, $27.14 < \sigma_\theta < 27.29$ kg/m³), and a lower AAIW (AAIW-L, $27.29 < \sigma_\theta < 27.35$ kg/m³). The AAIW-U and AAIW-C are classified as Subantarctic Mode Water (SAMW, Provost et al., 1995). Underneath the AAIW, Upper Circumpolar Deep Waters (UCDW) correspond to potential density between 27.35 and 27.73 kg/m³. The std in salinity and density show a local maximum at the interface between the AAIW and UCDW at depth of 34.25 and 34.32 psu isohaline and 27.3 and 27.35 kg/m³ isopycnals (Figures 6f and 6g). The depth of AAIW-UCDW interface varies over a range of 200 m. In contrast, the std of potential temperature decreases monotonically with depth as AAIW and UCDW have similar temperatures (between 2.7°C and 2.5°C) (Figure 6a). The range in Θ /S delimiting the AAIW-UCDW interface is shaded in Figure 6i.

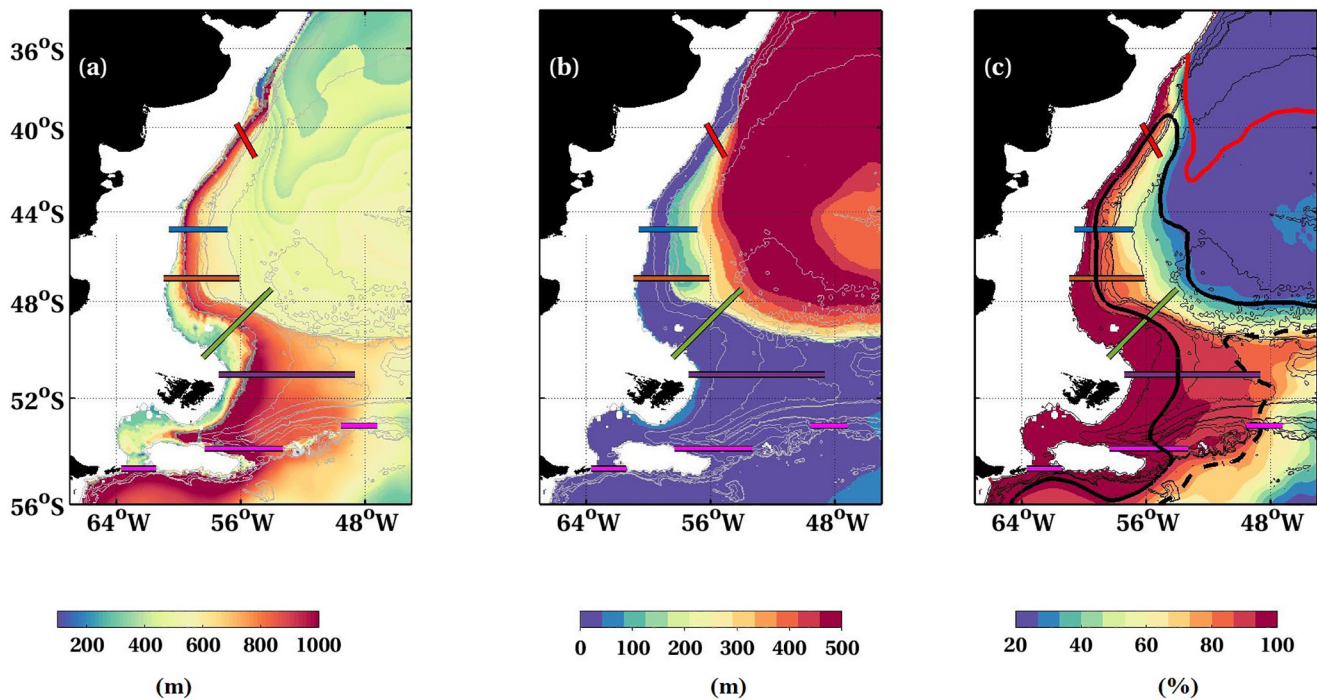


Figure 7. (a) Mean thickness (in m) of MUW layer (waters with $\Theta_{\text{mean}} > 2.5^{\circ}\text{C}$ and $33.9 < S_{\text{mean}} < 34.32$ psu) (b) Mean depth (in m) of the upper boundary of the MUW layer (c) Presence probability of MUW over upper 900 m. 100% means that these waters occupy the whole upper 900 m all the time. Black solid and dashed contour indicate the position of the Subantarctic Front and Polar Front and the red contour the position of the Subtropical Front.

4.1. Spatial Distribution of the SASW and AAIW Layer (Malvinas Upper Waters)

We focused on SASW and AAIW called hereafter MUW (for Malvinas Upper Waters). Θ/S criteria (in the range of the shaded area in Figure 6i) were used to define the lower boundary of the MUW layer. On average, the MUW occupy a thick layer (>800 m) reaching the surface along the Patagonian slope and Malvinas Plateau, and, a thinner layer isolated from the surface offshore (Figures 7a and 7b). The thin layer in the subtropical gyre (<300 m) is found at depth below 800 m and corresponds to eroded AAIW with Indian Ocean influence recirculating southward (Gordon et al., 1992; Maamaatuaiahutapu et al., 1998).

We computed the presence probability of the MUW in the upper 900 m over the 25 years (Figure 7c): 100% means that these waters occupy the upper 900 m all the time. The MUW are mostly common ($>90\%$ of occurrences) in the upper 900 m at EBB and all along the Patagonian continental slope south of 38°S (Figure 7c). The MUW water flow occurs primarily in a narrow band closely following the continental slope.

4.2. Modification Through Winter Convection

We investigate MUW modification through deep mixed layer formation. Two mixed-layer depth (MLD) definitions, one based on potential density and the other on turbocline (de Boyer Montegut et al., 2004), provided similar results. Large winter MLDs occur over the western portion of the Malvinas Plateau reaching 300 m in August on average over 25 years (Figure 8a) and maximum values of 600 m (Figure 8b). Winter mixing convection contributes to the regular outcropping of 27 and 27.1 kg/m^3 isopycnals over the Malvinas Plateau (Figure 8c). During some winters, water as dense as 27.10 kg/m^3 is found at the surface as north as 44°S . The maps of potential density maxima at the surface from GLORYS12 are consistent with maps of 27.10 and 27.20 kg/m^3 isopycnal depths constructed from winter data collected in 1980 (Piola & Gordon, 1989).

The winter MLD and surface potential density over the Malvinas Plateau undergo large interannual variations as illustrated at 51°S over the 1,500 m isobath (Figure 8e). Although the MLD time series mimics the surface potential density time series, the deepest MLDs do not always correspond to the largest surface

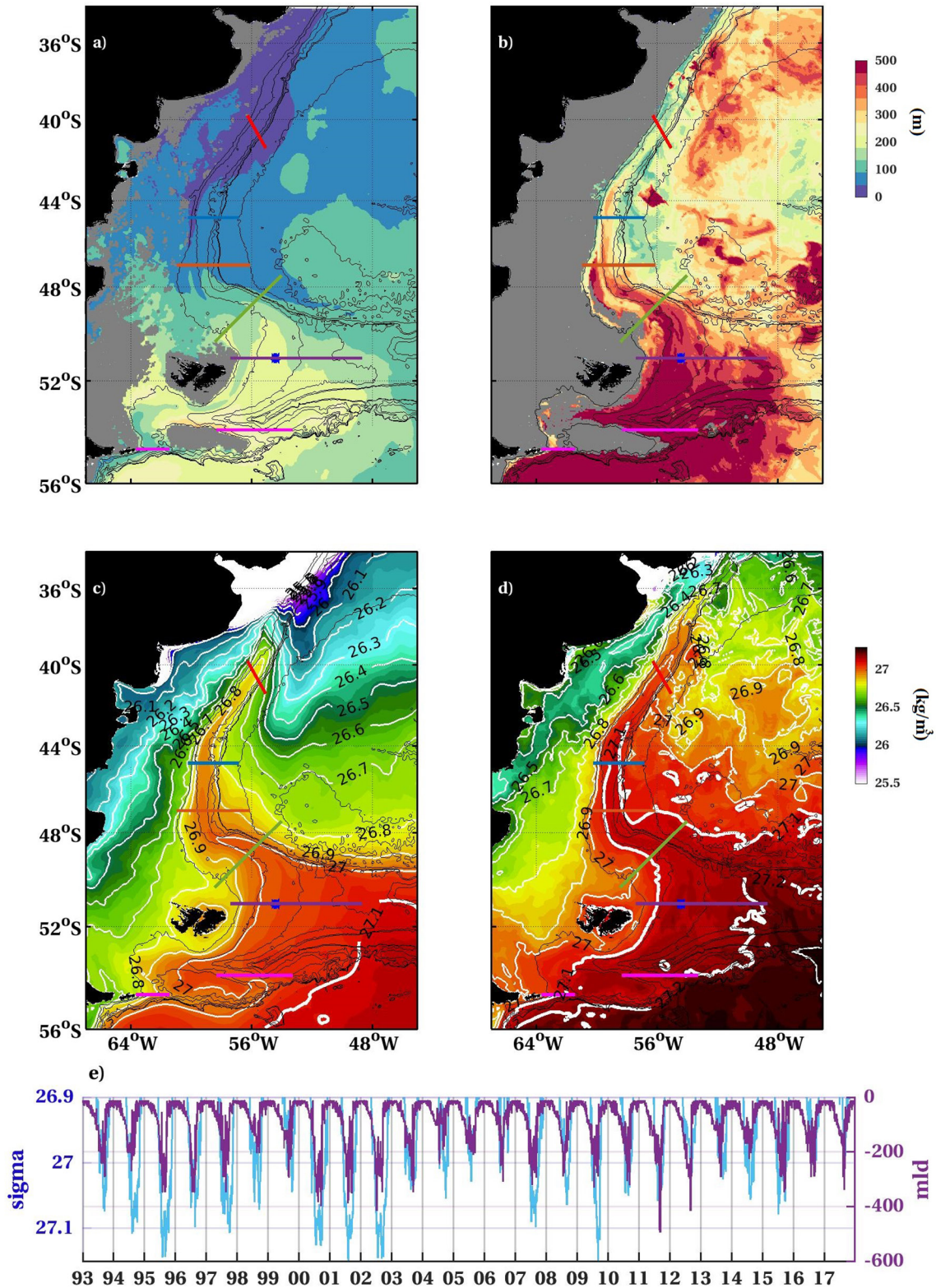


Figure 8. Mean (a and c) and maximum (b and d) mixed layer depth (in m) and surface potential density in August. Gray colors indicate regions where the MLDs reach the bottom (e) Mixed layer depth (purple in m) and potential density (in kg/m^3) time series above the Malvinas Plateau at the blue point indicated in (a–c).

density values as other processes contribute to modify density in winter (e.g., eddy mixing, lateral fluxes). The potential density and MLD time series suggest a low frequency modulation (e.g., deep MLD observed in 95–97, 00–02, and 11–12) (Figure 8e). August 2011 registered the deepest (500 m) MLD of the time series. Contrasted synoptic situations in January and August 2011 (Figure 9) along section 51°S illustrate processes at stake on the Plateau and are compared to the mean (Figure 6).

4.3. Modification of Water Properties on the Malvinas Plateau

Synoptic Sea Surface Height maps (Figures 9a and 9f) show an exacerbated mesoscale field compared to the rather smoothed mean field (Figure 6j). The Frontal Zone region (between the SAF-M and PF-N), which corresponds to the large deep reaching velocity std values (Figure 6h), is filled with energetic eddies and meanders leading to active stirring of properties. Indeed, the temperature and salinity fields in the Frontal Zone are drastically different from the smooth means (Figures 9b, 9c, 9g, and 9h) to be compared with Figures 6a and 6b) with intrusions of cold and fresh water in the upper 500 m. For example, the 34.05 psu isohaline that is confined near the surface in the mean field deepens down to 450 m (km 450 in Figure 9b) while the 3°C isotherm rises by 700 m in January (between km 200 and 400 in Figure 9c), which is consistent with the large std values (Figures 6e and 6f). The spectacular change in the Θ -S diagram between January and August (Figures 9e and 9j) reflects the winter convection that reaches the 27.1 kg/m³ σ_θ -horizon ventilating the AAIW-U. Indeed, the MLD changes from 10 m in January (strong summer thermocline) to over 500 m in August in the SAF region.

Selected Θ -S profiles in January show two changes in the slope of the Θ -S distribution between the 27.0 and 27.1 kg/m³ isopycnals (e.g., green profile in Figure 9e). They illustrate the lateral exchanges in the Frontal Zone where the cool and fresh waters from the PF encounter the warmer and salty waters from the west of the SAF. In August the change in slope in the Θ -S distribution located on the 27.15 kg/m³ σ_θ -horizon is associated to a profile within a meander of the PF (red profile in Figure 9j). These polar waters will eventually contribute to the freshening and cooling in the Frontal Zone in the upper 500 m and the change in slope will migrate to a lighter horizon (as seen in January).

5. MUW Volume Transports

MUW volume transports at each time step were estimated using Θ /S criteria in the range defined in Figure 6i ($\Theta > \Theta_0$ and $33.9 < S < S_0$ with Θ_0 varying between 2.5 and 2.7°C and S_0 between 34.25 and 34.32). Sensitivities to the temperature and salinity criteria, to the length of the sections were carefully examined using different Θ /S thresholds, extending sections toward the east and, considering positive only (T+) and all velocities (T±) (see supplementary material S6). We also checked the impact of trends in water properties. Indeed, over the slope south of 40°S and Malvinas Plateau, rather large freshening trends (with values 0.1, 0.08, and 0.04 psu/decade at 50, 155, and 541 m, respectively) lead to density decreases of about 0.05 kg/m³/decade while temperature trends are small (supplementary material S6). However, the 34.25/34.32 psu isohalines remained roughly at the same place (slightly deepening and larger vertical salinity gradient) and therefore the bottom limit of the MUW did not change much. The results were robust, yielded highly correlated transport time series ($r > 0.7$), means within a range of 6 Sv and stds within a range of 3 Sv. The relative uncertainty of the mean transport was of the order of 16% for (T±) (means within a 6 Sv range) and reduced to 5% (means within a 1.5 Sv range) for (T+). Hereafter, we discuss MUW transport computed from positive velocities in the layer defined by $\Theta > 2.5^\circ\text{C}$ and $33.9 < S < 34.25$ psu. The MUW transport time series (T+) and (T±) are shown in supplementary material (S5) and their statistics summarized in Table 3.

5.1. The Malvinas Upper Water Transport

The northward MUW transport means decrease toward the north from 31 Sv at 51°S to 27 Sv at 41°S indicating offshore leakage and mixing (Figure 10a). The transport std decreases from 4.6 Sv at 51°S to 3.4 Sv at 44°S and shows larger values at 41°S near the Confluence (5 Sv) and at 59°W (5 Sv) near the blocking region (Figure 2b) where the offshore side of the sections reaches a large EKE region (Figure 1c). MUW transport time series (daily resolution) from different latitudes are significantly correlated and maximum correlations between sections are obtained at small lags (<5 days) (Table 2). The smallest correlations are found with

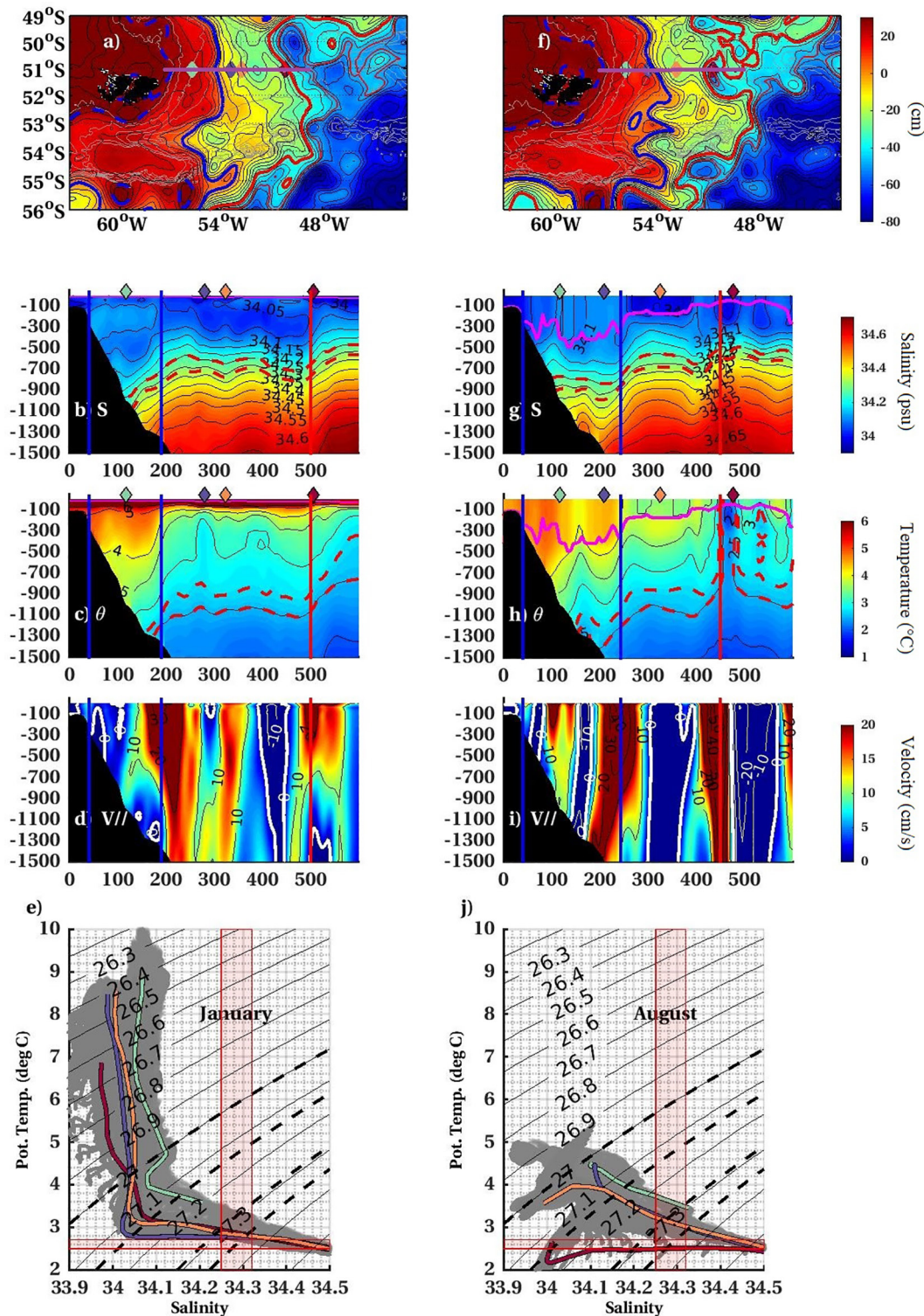


Figure 9. (a) Sea Surface Height map of January 2, 2011. The position of the SAF-M/SAF-N and PF-N/PF-M are indicated in blue and red. The 500, 1,000, 1,500, 2,000, and 2,500 m isobaths are indicated in gray. (b–d): Salinity, Temperature and along slope velocities over the 51°S section indicated in purple in Figure (a) The 2.5°C and 2.7°C isotherms and the 34.32 and 34.25 psu isohaline are indicated with dashed red contour. The MLD is indicated with a pink contour. (e) θ -S diagram from January 2011 over the 51°S section indicated in purple in (a) The vertical rectangle marks 34.25 and 34.32 psu values and the horizontal rectangle the 2.5°C and 2.7°C values. In colors selected profiles from 2 January. The location of each profile is indicated with colored diamonds in a-f. (j) same for August 2011. The selected profiles are from the August 31, 2011.

Table 3
Statistics for MUW Transport Computed Considering Positive ($T+$) and Both Sign Velocities ($T\pm$) Across 5 Sections Crossing the MC at 41°S, 44.7°S, 47°S, 59°W, and 51°S and 3 Sections at North Scotia Ridge: At EBB, WBB, and SRP (Location Indicated in Figure 1c)

Section	Volume transports $T+/T\pm$				r
	Mean (Sv)	Std (Sv)	Max (Sv)	Min (Sv)	
41°S	27/23	5/7	48/48	1/-6	0.86
44.7°S	28/23	3/5	42/39	13/-0.9	0.71
47°S	30/27	4/4	47/46	14/7	0.87
59°W	31/25	5/8	57/57	12/-3	0.84
51°S	31/27	4/4	53/44	18/7	0.74
EBB	20/17	6/4	41/35	6/4	0.90
SRP	15/15	4/6	40/40	0/4	0.99
WBB	2/1	0.9/0.7	6/5	0.3/-1	0.87
EBB +SRP+WBB	38/34	7/6	63/59	17/9	0.94

The correlation coefficient (r) between transport time series computed from $T+$ and $T\pm$ is reported in the last column.

the 41°S, 59°W, and 51°S sections which receive perturbations from the Confluence, from blocking/feeding events and, from Drake Passage, respectively (Figure 2) locally affecting the transport. Correlations between MUW transport time series at different latitudes are larger (>0.2) than those obtained for the upper 900 m transport time series (Table 2).

The five MUW transport time series do not exhibit much variation at the seasonal time scale (small increase of 2 Sv in winter in all sections, Figure 10b) and no long-term trend. Annual means vary over a range of about 6 Sv. The annual means show a decrease in 2004 in the five sections (from 3 to 7 Sv). The 2004 transport minimum is examined below.

5.2. Comparison to Upper 900 m Transport

We compared the MUW transport (integrated in the layer defined by $\Theta > 2.5^\circ\text{C}$ and $33.9 < S < 34.25$ psu) at 44.7°S and 47°S to the MC transport without water mass distinction, integrated in the first 900 m (Figures 11a and 11b). The std and mean transport considering the first 900 m is larger than the MUW transport (mean of 37 and 42 Sv and stds of 4 and 4.8 Sv at 44.7°S and 47°S, respectively).

The MUW and the 900 m volume transport time series are correlated ($r > 0.8$ above the 99% confidence level). However, at specific events they show an opposite behavior with the 900 m transport experiencing an increase and the MUW transport a drastic decrease (e.g., year 1995, 2004 end of 2011 in Figures 11a and 11b). The dates of large difference correspond to feedings events of the MC when Polar waters are supplied to the offshore side of the MC as the PF-N meanders northward (Figures 2b, 11c and 11d, Artana, Lellouche, Sennechael, et al., 2018). Indeed, polar waters are not considered in the MUW transport computation leading to a decrease in the MUW transport while the PF-N cyclonic meander of the PF-N tends to accelerate the offshore MC flow leading to an increase in the 900 m transport. The transport differences are larger during years 93–97 and 04–17 in agreement with increased occurrence of feeding events during these periods (Figures 11c and 11d). In contrast, transport differences reduce during blocking events (Figure 2b) as the anticyclonic anomalies obstructing the MC flow at 49°S carry warm and salty waters that are not included in the MUW transport computation (Figures 11c and 11d).

Year 2004 stands out with prolonged feeding events and two blocking events in March and October (Figures 11c and 11d). The feeding and blocking events lasted 30 and 40 days and were associated with density anomalies of $+0.08 \text{ kg/m}^3$ and -0.13 kg/m^3 , respectively. This year corresponds to a notable decrease in the MUW annual mean transports at all latitudes (Figure 10c) while the 900 m annual mean transport is 0.5 Sv larger than the mean (not shown). In year 2004, the South Atlantic Subtropical High was located to the southwest of its mean location (Figure 12a) and a large southward intrusion of salty and warm subtropical waters into the Argentine Basin occurred (Figure 12b). As a result, salinity increased by more than 0.2 psu at the surface and 0.1 psu at 541 m in the western Argentine Basin (Figures 12c and 12e). In particular, waters saltier than 34.25 psu reached the offshore side of the northern sections (41°S, 44°S, and 47°S) on several occasions (Figure 12d) and, in March and October generated two blocking events on the 59°W section (not shown).

All over the Patagonian slope waters were 0.1 psu fresher at the surface and 0.1 saltier at 541 m as a result of the prolonged feeding events (Figures 12b–12e). The salty (>34.25 psu) waters from the blocking and feeding (delimited with red in Figures 12b and 12d) events are excluded from the computation of the MUW transport, explaining the decrease in the annual means in 2004 (Figure 10c).

Interestingly, the feeding events contributed to increase the stratification in the southern part of the MC thereby probably leading to the minimum observed in the winter MLD in 2004 (Figure 8e).

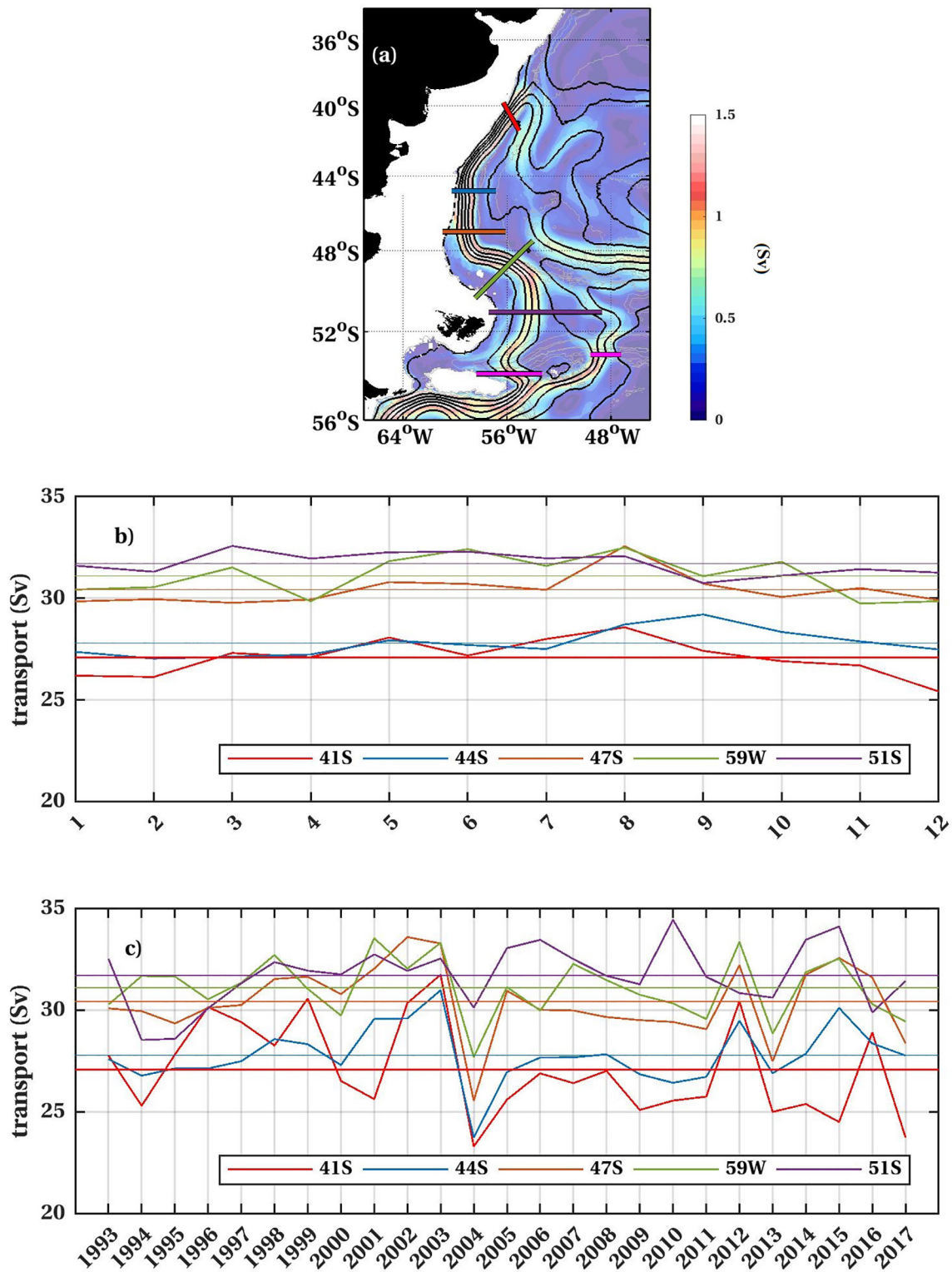


Figure 10. (a) Stream function of the mean volume transport associated to the MUW layer ($\Theta > 2.5^{\circ}\text{C}$ and $33.9 < S < 34.25$ psu). Background is mean volume transport in each model grid (in Sv) and isolines are plotted every 5 Sv. Monthly (b) and yearly (c) averages of MUW volume transport (in Sv) along five sections in the MC.

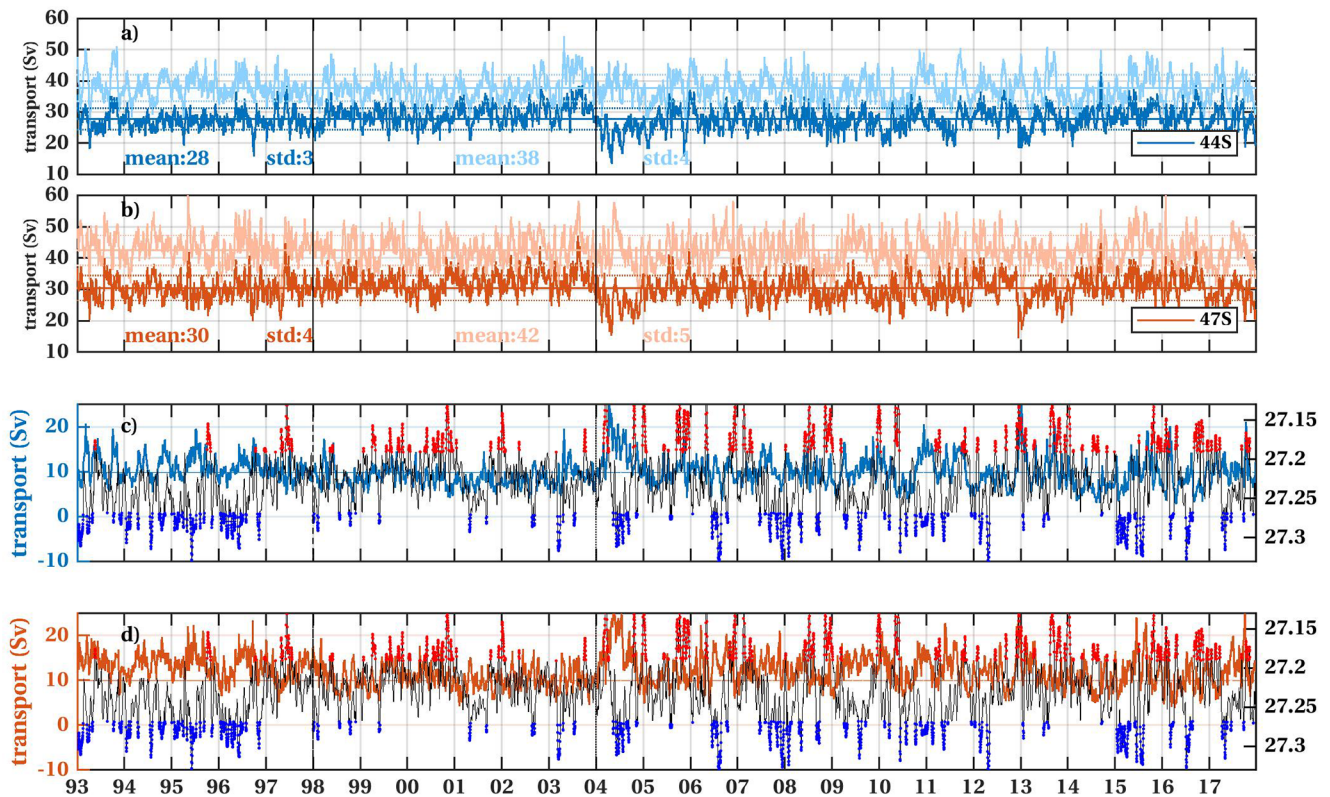


Figure 11. Volume transport time series across the MC at (a) 44.7°S and (b) 47°S. Dark-colored timeseries correspond to MUW volume transport and light-colored time series to the volume transport integrated over the upper 900 m. Difference between the two transport time series at 44.7°S in blue (c) and 47°S in orange (d). Superimposed in black is the time series of potential density at 541 m averaged over the yellow box in Figure 12d. Densities larger than the std in blue indicate feeding while densities lower than the std in red indicate blocking events (Artana, Lellouche, Sennechael, et al., 2018c).

6. Summary and Discussion

This work builds upon previous works that assessed GLORYS12 skills in the upper layer in the Southwestern Atlantic Ocean. We used 25 years of GLORYS12 ocean reanalysis to revisit the upper MC along its path from Drake Passage to the Brazil-Malvinas Confluence from synoptic to interannual time scales. In the upper 900 m, the MC carries Subantarctic Surface Waters and Antarctic Intermediate Water (we called them, Malvinas Upper Waters, MUW) and some Upper Circumpolar Deep Waters.

The MC is a rather steady current connecting two regions with high eddy kinetic energy (Drake Passage and the Brazil-Malvinas Confluence) as most of the EKE leaking from Drake Passage is damped over the Malvinas Plateau. Indeed, The Malvinas Plateau is a hotspot region for eddy activity dissipation (Artana et al., 2016, Figure 2a), and for local water mass properties modification either through eddy mixing or through winter convection (Figure 13a). On the Malvinas Plateau, deep winter mixed layers attain on average a depth of 300 m and occasionally reach 600 m. Deep mixed layers reach density values as large as 27.1 kg/m³, ventilating the AAIW-U as observed in Piola and Gordon (1989).

The upper 900 m transport mean decreases from 40 Sv at 51°S to 35 Sv at 41°S indicating offshore leakage along the MC path. At 51°S the upper MC volume transport (40 Sv) receives a mean contribution of 3 Sv from WBB, 23 Sv from EBB and 14 Sv from SRP.

Computing MC transport time series at different latitudes requires care because the choice of the eastern limit of the section, embedded in large EKE regions, impacts on the transport time series variations. Transport time series in the upper 900 m and in the MUW layer were produced considering positive ($T+$) and both sign velocities ($T\pm$) to take into account the difficulties associated with the open eastern boundary. The mean MUW transport is not very sensitive to the different Θ/S criteria used (in the range defined by $\Theta > \Theta_0$ and $33.9 < S < S_0$ with Θ_0 varying between 2.5 and 2.7°C and S_0 between 34.25 and 34.32) while the relative

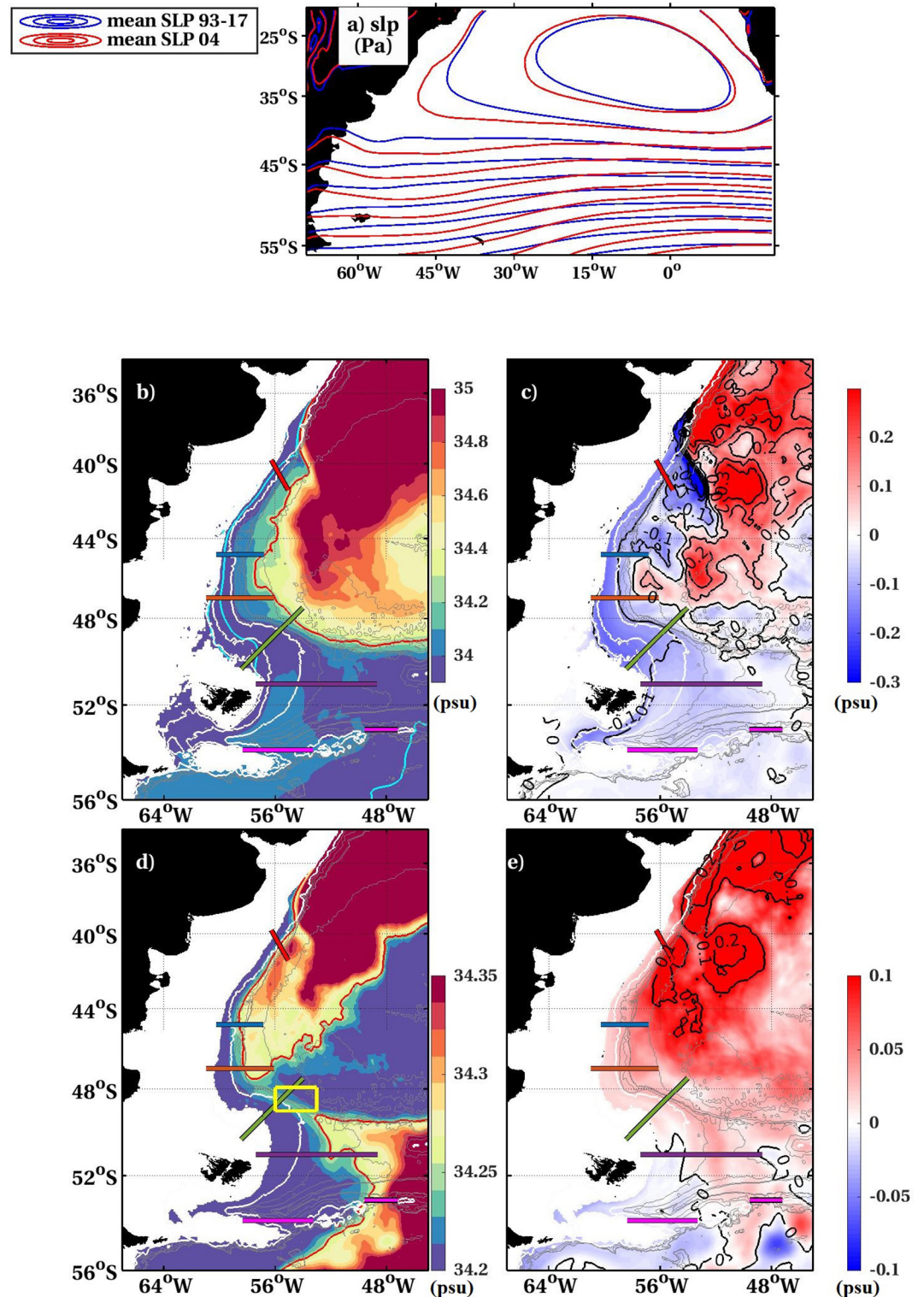


Figure 12. (a) Mean Sea Level Pressure contours averaged over 2004 (in red) and over the 25 years (in blue). (b and d) Mean salinity at the surface and 541 m over 2004. The cyan and red contour represent the mean position of the 33.9 and 34.25 psu isohalines. (c and e) Salinity anomaly at the surface and 541 m over 2004. Indicated are five sections along the MC and three sections across North Scotia Ridge and a yellow box in (d) over which spatially averaged time series of potential density are computed (shown in Figures 11c and 11d).

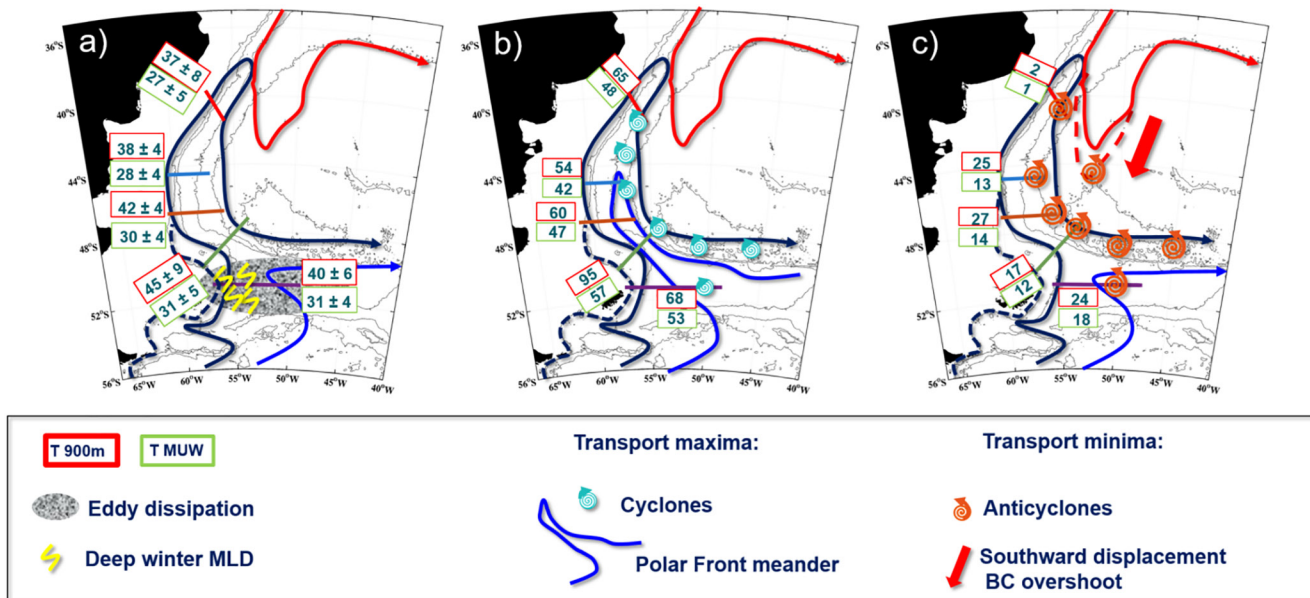


Figure 13. Schematics of MC transports and physical processes. (a) The mean and std of the upper 900 m transports ($T+ 900\text{ m}$) and the MUW transports ($T+ \text{ MUW}$) are indicated in red and green boxes. The Malvinas Plateau is home to active eddy mixing, eddy dissipation and deep winter mixed layers occasionally reaching 600 m depth (yellow). (b) Synoptic transport maxima correspond either to polar front meanders or to cyclones. (c) Synoptic transport minima are associated with anticyclones. The southward migration of the Brazil Current overshoot (red arrow) led to an increase of mesoscale activity south of 44°S.

uncertainty reduces from 16% in MUW ($T\pm$) to 5% in the MUW ($T+$). The 900 m volume transport and the MUW transport are correlated (>0.8) and show little seasonality (relative seasonal std of 2%) and no trend. Differences between the upper 900 m transport and the MUW transport are modulated by the occurrence of feeding events and blocking events. Indeed, waters advected during blocking events (salty and warm in the upper layer) and feeding events (fresh at the surface and salty at depth) are excluded from the computation of the MUW transport. The 2004 MUW transport minimum (reduction of 5 Sv) was associated with a unique southward displacement of the BC overshoot, blocking events at 48°S and a prolonged feeding event.

Synoptic transport maxima in the upper 900 m are associated either to feeding events in the South or cyclonic eddies propagating north or local mesoscale activity at the Confluence (Figure 13b). As cyclones with polar waters do not contribute to the MUW transport, the MUW maxima are not necessarily simultaneous with the upper 900 m transport maxima (Figure 13b). Drastic reductions in the upper 900 m and MUW transport occurred at the Confluence and at 59°W during blocking events (Figure 13c). Over the 25 years, 100 blocking events and 96 feeding events occurred at 59°W. Blocking events at 59°W became more frequent over the last decade (35 during 93-05 and 65 during 05-17). The southward displacement of the BC overshoot could contribute to that increase (Figure 13c). However, the origin of the perturbations leading to the blocking events remains uncertain. Backward trajectories of lagrangian particles did not lead to conclusive results: tracking back anomalies in the Argentine Basin is difficult because of the intense mesoscale activity. It is possible that events of transport reductions as the one in 2004 will be more frequent in the future.

Overall the MC is a strong and steady current. The standard deviation of the transport is small relative to the mean: about 10% at 44.7°S and 47°S and 20% at 41°S near the Confluence, 59°W in the blocking region and 51°S on the Malvinas Plateau. In contrast, the ratio std/mean of the BC transport is of the order of 57% at 37°S (Artana, Provost, et al., 2019). The MC plays a minor role in the velocity variations observed at the confluence at seasonal and interannual scales. Velocity trends are small over the MC while they are large at the Brazil Malvinas Confluence and the overshoot (10 cm/s/decade at the surface) as the BC migrated southward over the last 25 years.

Estimates of total volume transport provide values (70–45 Sv from south to north) that are in agreement with the few existing estimates based on observations (Colin de Verdière & Ollitraul, 2016; Maamaatuaiahutapu et al., 1998; Peterson, 1992; Saunders & King, 1995). Deep Argo floats deployed in the Southern Ocean will be examined to precisely evaluate the water mass characteristics and velocities at depths in GLORYS12. Furthermore, on-going efforts aim at providing a new ocean reanalysis with the number of vertical levels increasing from 50 to 75 and assimilating deep Argo floats. These improvements will probably provide further insights on deep circulation and water masses.

Data Availability Statement

The model outputs are available at Copernicus Marine Environment Monitoring Service (CMEMS; <http://marine.copernicus.eu/>).

Acknowledgments

We are grateful to the CNES (Centre National d'Etudes Spatiales) for constant support. This study is a contribution to EUMETSAT/CNES DSP/OT/12–2118. Léa Poli acknowledges support from Sorbonne Université and Camila Artana from a CNES Postdoc Scholarship.

References

- Artana, C., Ferrari, R., Bricaud, C., Lellouche, J.-M., Garric, G., Sennéchaël, N., et al. (2019). Twenty-five years of Mercator ocean reanalysis GLORYS12 at Drake Passage: Velocity assessment and total volume transport. *Advances in Space Research*. <https://doi.org/10.1016/j.asr.2019.11.033>
- Artana, C., Ferrari, R., Koenig, Z., Saraceno, M., Piola, A. R., & Provost, C. (2016). Malvinas Current variability from Argo floats and satellite altimetry. *Journal of Geophysical Research: Oceans*, *121*, 4854–4872. <https://doi.org/10.1002/2016JC011889>
- Artana, C., Ferrari, R., Koenig, Z., Sennéchaël, N., Saraceno, M., Piola, A. R., & Provost, C. (2018). Malvinas Current volume transport at 41°S: A 24 yearlong time series consistent with mooring data from 3 decades and satellite altimetry. *Journal of Geophysical Research: Oceans*, *123*, 378–398. <https://doi.org/10.1002/2017JC013600>
- Artana, C., Lellouche, J. M., Park, Y. H., Garric, G., Koenig, Z., Sennéchaël, N., et al. (2018). Fronts of the Malvinas Current system: surface and subsurface expressions revealed by satellite altimetry, Argo floats, and Mercator operational model outputs. *Journal of Geophysical Research: Oceans*, *123*, 5261–5285. <https://doi.org/10.1029/2018JC013887>
- Artana, C., Lellouche, J.-M., Sennéchaël, N., & Provost, C. (2018). The open-ocean side of the Malvinas Current in Argo floats and 24 years of mercator ocean high-resolution (1/12) physical reanalysis. *Journal of Geophysical Research: Oceans*, *123*, 8489–8507. <https://doi.org/10.1029/2018JC014528>
- Artana, C., Provost, C., Lellouche, J. M., Rio, M. H., Ferrari, R., & Sennéchaël, N. (2019). The Malvinas Current at the Confluence with the Brazil Current: Inferences from 25 years of Mercator Ocean reanalysis. *Journal of Geophysical Research: Oceans*, *124*, 7178–7200. <https://doi.org/10.1029/2019JC015289>
- Barré, N., Provost, C., & Saraceno, M. (2006). Spatial and temporal scales of the Brazil-Malvinas Current confluence documented by simultaneous MODIS Aqua 1.1-km resolution SST and color images. *Advances in Space Research*, *37*(4), 770–786. <https://doi.org/10.1016/j.asr.2005.09.026>
- Boyer Montegut, C., Madec, G., Fischer, A. S., Lazar, A., & Iudicone, D. (2004). Mixed layer depth over the global ocean: An examination of profile data and a profile-based climatology. *Journal of Geophysical Research*, *109*, C12003. <https://doi.org/10.1029/2004JC002378>
- Cabanes, C., Grouazel, A., von Schuckmann, K., Hamon, M., Turpin, V., Coatanoan, C., et al. (2013). The CORA dataset: Validation and diagnostics of in-situ ocean temperature and salinity measurements. *Ocean Science*, *9*(1), 1–18. <https://doi.org/10.5194/os-9-1-2013>
- Colin de Verdière, A., & Ollitraul, M. (2016). A Direct Determination of the World Ocean Barotropic Circulation. *Journal of Physical Oceanography*, *46*, 255–273. <https://doi.org/10.1175/jpo-d-15-0046.1>
- Frey, D. I., Piola, A. R., Krechik, V. A., Fofanov, D. V., Morozov, E. G., Silvestrova, K. P., et al. (2021). Direct measurements of the Malvinas Current velocity structure. *Journal of Geophysical Research: Oceans*, *126*, e2020JC016727. <https://doi.org/10.1029/2020JC016727>
- Gordon, A. L., & Greengrove, C. L. (1986). Geostrophic circulation of the Brazil-Falkland Confluence. *Deep-Sea Research Part A: Oceanographic Research Papers*, *33*, 573–585. [https://doi.org/10.1016/0198-0149\(86\)90054-3](https://doi.org/10.1016/0198-0149(86)90054-3)
- Gordon, A. L., Weiss, R. F., Smethie, W. M., & Warner, M. J. (1992). Thermocline and intermediate water communication between the South Atlantic and Indian Oceans. *Journal of Geophysical Research*, *97*, 7223–7240. <https://doi.org/10.1029/92JC00485>
- Lellouche, J.-M., Greiner, E., Le Galloudec, O., Garric, G., Regnier, C., Drevillon, M., et al. (2018). Recent updates on the Copernicus Marine Service global ocean monitoring and forecasting real-time 1/12° high resolution system. *Ocean Science Discussions*. <https://doi.org/10.5194/os-2018-1510.17125/gov2018.ch20>
- Lellouche, J.-M., Le Galloudec, O., Drévillon, M., Régnier, C., Greiner, E., Garric, G., et al. (2013). Evaluation of real time and future global monitoring and forecasting systems at Mercator Ocean. *Ocean Science Discussions*, *9*, 1123–1185. <https://doi.org/10.5194/osd-9-1123-2012>
- Maamaatuaiahutapu, K., Garçon, V. C., Provost, C., Boulahtid, M., & Bianchi, A. A. (1994). Spring and winter water mass composition in the Brazil-Malvinas Confluence. *issn: 0022-2402*, *52*, 397–426. <https://doi.org/10.1357/0022240943077064>
- Maamaatuaiahutapu, K., Garçon, V. C., Provost, C., & Mercier, H. (1998). Transports of the Brazil and Malvinas Currents at their Confluence. *Journal of Marine Research*, *56*, 417–438. <https://doi.org/10.1357/002224098321822366>
- Mulet, S., Rio, M.-H., Etienne, H., Artana, C., Cancet, M., Dibarbouré, G., et al. (2020). The new CNES-CLS18 Global Mean Dynamic Topography. *Ocean Science*. <https://doi.org/10.5194/os-2020-117>
- Paniagua, G. F., Saraceno, M., Piola, A. R., Guerrero, R., Provost, C., Ferrari, R., et al. (2018). Malvinas Current at 40°S–41°S: First assessment of temperature and salinity temporal variability. *Journal of Geophysical Research: Oceans*, *123*, 5323–5340. <https://doi.org/10.1029/2017JC013666>
- Peterson, R. G. (1992). The boundary currents in the western Argentine Basin. *Deep-Sea Research Part A*, *39*(3–4), 623–644. [https://doi.org/10.1016/0198-0149\(92\)90092-8](https://doi.org/10.1016/0198-0149(92)90092-8)
- Peterson, R. G., & Whitworth, T. (1989). The subantarctic and polar fronts in relation to deep water masses through the southwestern Atlantic. *Journal of Geophysical Research*, *94*(C8), 10817–10838. <https://doi.org/10.1029/JC094iC08p10817>

- Piola, A. R., Franco, B. C., Palma, E. D., & Saraceno, M. (2013). Multiple jets in the Malvinas Current. *Journal of Geophysical Research: Oceans*, *118*, 2107–2117. <https://doi.org/10.1002/jgrc.20170>
- Piola, A. R., & Gordon, A. L. (1989). Intermediate waters in the southwest South Atlantic. *Deep-Sea Research Part A. Oceanographic Research Papers*, *36*(1), 1–16. [https://doi.org/10.1016/0198-0149\(89\)90015-0](https://doi.org/10.1016/0198-0149(89)90015-0)
- Poli, L., Artana, C., Provost, C., Sirven, J., Sennéchaël, N., Cuyper, Y., & Lellouche, J.-M. (2020). Anatomy of subinertial waves along the Patagonian shelf break in a 1/12° global operational model. *Journal of Geophysical Research: Oceans*, *125*, e2020JC016549. <https://doi.org/10.1029/2020jc016549>
- Provost, C., Gana, S., Garçon, V., Maamaatuaiahutapu, K., & England, M. (1995). Hydrographic conditions in the Brazil-Malvinas Confluence during austral summer 1990. *Journal of Geophysical Research*, *100*(C6), 10655–10682. <https://doi.org/10.1029/94JC02864>
- Pujol, M.-L., Faugère, Y., Taburet, G., Dupuy, S., Pelloquin, C., Ablain, M., & Picot, N. (2016). DUACS DT2014: The new multi-mission altimeter data set reprocessed over 20 years. *Ocean Science*, *12*(5), 1067–1090. <https://doi.org/10.5194/os-12-1067-2016>
- Romero, S. I., Piola, A. R., Charo, M., & Garcia, C. A. E. (2006). Chlorophyll-a variability off Patagonia based on SeaWiFS data. *Journal of Geophysical Research*, *111*, C05021. <https://doi.org/10.1029/2005JC003244>
- Saraceno, M., Provost, C., Piola, A. R., Gagliardini, A., & Bava, J. (2004). Brazil Malvinas Frontal System as seen from 9 years of advanced very high resolution radiometer data. *Journal of Geophysical Research*, *109*, C05027. <https://doi.org/10.1029/2003JC002127>
- Saraceno, M., Provost, C., Piola, A. R., Guerrero, R., Ferrari, R., Paniagua, G. F., et al. (2020). Malvinas Current 2015–2017: Mooring velocities. *SEANOE*. <https://doi.org/10.17882/76617>
- Saunders, P. M., & King, B. A. (1995). Bottom Currents Derived from a Shipborne ADCP on WOCE Cruise A11 in the South Atlantic. *Journal of Physical Oceanography*, *25*, 329–347. [https://doi.org/10.1175/1520-0485\(1995\)025<0329:bcdfas>2.0.co;2](https://doi.org/10.1175/1520-0485(1995)025<0329:bcdfas>2.0.co;2)
- Smith, W. H. F., & Sandwell, D. T. (1994). Bathymetric prediction from dense satellite altimetry and sparse shipboard bathymetry. *Journal of Geophysical Research*, *99*, 21803–21824. <https://doi.org/10.1029/94JB00988>
- Spadone, A., & Provost, C. (2009). Variations in the Malvinas Current volume transport since October 1992. *Journal of Geophysical Research*, *114*, C02002. <https://doi.org/10.1029/2008JC004882>
- Szekeley, T., Gourrion, J., Pouliquen, S., & Reverdin, G. (2016). CORA, Coriolis, Ocean Dataset for Reanalysis. SEANOE. <https://doi.org/10.1029/2008JC05248>
- Valla, D., & Piola, A. R. (2015). Evidence of upwelling events at the northern Patagonian shelf break. *Journal of Geophysical Research: Oceans*, *120*, 7635–7656. <https://doi.org/10.1002/2015JC011002>
- Vivier, F., & Provost, C. (1999a). Direct velocity measurements in the Malvinas Current. *Journal of Geophysical Research*, *104*, 21083–21103. <https://doi.org/10.1029/1999JC900163>
- Vivier, F., & Provost, C. (1999b). Volume transport of the Malvinas Current: Can the flow be monitored by TOPEX/Poseidon? *Journal of Geophysical Research*, *104*, 21105–21122. <https://doi.org/10.1029/1999JC900056>

References From the Supporting Information

- Böning, C. W., Dispert, A., Visbeck, M., Rintoul, S. R., & Schwarzkopf, F. U. (2008). The response of the Antarctic Circumpolar Current to recent climate change. *Nature Geoscience*, *1*(12), 864–869. <https://doi.org/10.1038/ngeo362>
- Close, S. E., Naveira Garabato, A. C., McDonagh, E. L., King, B. A., Biuw, M., & Boehme, L. (2013). Control of mode and intermediate water mass properties in Drake Passage by the Amundsen Sea low. *Journal of Climate*, *26*(14), 5102–5123. <https://doi.org/10.1175/jcli-d-12-00346.1>
- Naveira Garabato, A. C., Jullion, L., Stevens, D. P., Heywood, K. J., & King, B. A. (2009). Variability of subantarctic mode water and Antarctic intermediate water in the Drake Passage during the late-twentieth and early-twenty-first centuries. *Journal of Climate*, *22*(13), 3661–3688. <https://doi.org/10.1175/2009JCLI2621.1>
- Purich, A., England, M. H., Cai, W., Sullivan, A., & Durack, P. J. (2018). Impacts of Broad-Scale Surface Freshening of the Southern Ocean in a Coupled Climate Model. *Journal of Climate*, *31*(7), 2613–2632. <https://doi.org/10.1175/JCLI-D-17-0092.1>